$\boldsymbol{V}$ = matrix of effective velocities (Part I, Eq. 21)
$\boldsymbol{V}_c$ = matrix of effective velocities in the constant coefficient axial dispersion model
$\boldsymbol{V}(\eta)$ = matrix of radially dependent velocities
V_{ye} = effective y-phase velocity when phase interactions are ignored

Greek Letters

ϵ = matrix of hold-up ratios
ζ = normalised axial coordinate
η = normalised radial coordinate
λ = Fourier transform variable
μ = viscosity
ρ = density
τ = dimensionless time
ω = matrix of weighting functions for concentration averaging

LITERATURE CITED

DeGance, A. E., and L. E. Johns, "The theory of dispersion of chemically active solutes in a rectilinear flow field," *Appl. Sci. Res.*, **34**, p. 189 (1978).

Dunn, W. E., T. Vermeulen, C. R. Wilke, and T. T. Word, "Longitudinal dispersion in packed gas-absorption columns," *Ind. Eng. Chem. Fund.*, **16**, p. 116 (1977).

Farid, M. M., and D. J. Gunn, "Dispersion in trickle and two-phase flow in packed columns," *Chem. Eng. Sci.*, **34**, p. 579 (1979).

Gill, W. N., and R. Sankarasubramanian, "Exact analysis of unsteady convective diffusion," *Proc. Roy. Soc.*, **A316**, p. 341 (1970).

Gill, W. N., and R. Sankarasubramanian, "Dispersion of a non-uniform slug in time-dependent flow," *Proc. Roy. Soc.*, **A322**, p. 101 (1971).

Hatton, T. A., "Mixing and mass transfer in the steady state absorption of carbon dioxide in a packed column," M.Sc. Thesis, Univ. Natal, Durban, South Africa (1976).

Hatton, T. A., and E. N. Lightfoot, "On the significance of the dispersion coefficient in two-phase flow," *Chem. Eng. Sci.*, **37**, p. 1289 (1982).

Hatton, T. A., and E. N. Lightfoot, "Dispersion, mass transfer and chemical reaction in multiphase contactors. I: Theoretical Developments," *AIChE J.* **30**, p. 235 (1984).

Hatton, T. A., and E. T. Woodburn, "Mixing and mass transfer at high liquid rates in the steady state counterflow operation of packed columns," *AIChE J.*, **24**, p. 187 (1978).

Linek, V., P. Benes, J. Sinkule, and Z. Krivsky, "Simultaneous determination of mass transfer coefficient and of gas and liquid dispersions and holdups in a packed absorption column by dynamic response method," *Ind. Eng. Chem. Fund.*, **17**, p. 298 (1978).

Subramanian, R. S., W. N. Gill, and R. A. Marra, "Dispersion models of unsteady tubular reactors," *Can. J. Chem. Eng.*, **52**, p. 563 (1974).

Woodburn, E. T., "A study of gas-phase axial mixing in a packed absorption tower," Ph.D. Thesis, Univ. Witwatersrand, Johannesburg, South Africa (1972).

Woodburn, E. T., "Gas phase axial mixing at extremely high irrigation rates in a large packed absorption tower," *AIChE J.*, **20**, p. 1003 (1974).

Manuscript received January 7, 1983; revision received May 5, and accepted May 10, 1983.

Experimental and Mathematical Modeling of Three-Dimensional Natural Convection in an Enclosure

Three-dimensional natural convection patterns in an enclosure under conditions simulating flow in glass-making furnaces have been calculated using an approximate method in which solutions for the temperature and velocity fields in orthogonal two-dimensional planes are superposed. The computational method was tested by comparison with measurements of the temperatures and velocities in an enclosure heated and cooled from above and with a controlled heat loss from the sides. Good agreement was found between measurements and computations under conditions of interest in glass-making furnaces, wherein the motion in one of the two orthogonal planes is dominant.

N. W. E. CURLET, K. J. WON, L. A. CLOMBURG, JR., and A. F. SAROFIM

Department of Chemical Engineering
Massachusetts Institute of Technology
Cambridge, MA 02139

SCOPE

Glass is produced by feeding a solid mixture consisting primarily of sodium carbonate and silica onto the surface of a glass melt. The solids float over the melt near their point of introduction to the furnace and are heated from below by the melt and from above by radiation from the flames and refractory. The heat transfer to the bottom surface of the floating solids is controlled by the natural circulation pattern which is driven by radiation from the flame to that portion of the melt not covered by the feed solids. The flow in the glass melt is predominantly two-dimensional, laminar and Newtonian, with a Rayleigh number of 10^6 to 10^8, and a Prandtl number of 200 to 5,000.

Numerical methods for solving natural convection patterns are well developed (Catton and Edwards, 1967; Mallison and de Vahl Davis, 1973; Ozoe et al., 1974) and have been applied with considerable success for determining the dominant two-dimensional motion in glass melts (Noble et al., 1972). Interest in obtaining the complete three-dimensional field has been motivated by the importance of flows in the plane orthogonal to that of the dominant flow; the flow in the transverse plane is needed for applications such as determining residence-time

Correspondence concerning this paper should be addressed to A. F. Sarofim.
N. W. E. Curlet and L. A. Clomburg, Jr. are currently with Shell Development Co., Houston, TX; K. J. Won with PPG Industries, Glass Research Center.

distribution, refractory wear, and effects on glass quality of changing side-wall insulation.

The determination of this three-dimensional motion is the subject of this paper. One part of the study is the measurement and calculation of the dominant two-dimensional flow and the extent to which it is affected by heat extraction in the transverse direction. Another part is the determination of the flow pattern in the transverse direction, which is affected both by heat losses through the side wall and energy transfer from the convective motion in the orthogonal plane.

CONCLUSIONS AND SIGNIFICANCE

The three dimensionality of the motion in simulated glass melts in which as much as 15% of the energy input is lost through the side walls has been characterized. The data in this study confirm the dominant two-dimensional motion previously reported by Clomburg (1971) and show that the basic characteristics of this flow are unaltered even when the side-wall heat loss is increased from less than 1 to 15% of the total heat input. The principal effects of these side-wall heat losses are to generate a boundary layer flow down the wall and reduce the temperature in the core. These effects can be predicted with surprising accuracy by using a two-dimensional numerical model in which allowance for three-dimensional effects is made with the use of distributed sources and sinks of energy.

In a more stringent test of the source-sink method, the predicted fields for the orthogonal transverse planes (where the source-sinks dominate the energy transfer) are in reasonable agreement with those measured.

The experimental results reported here reveal a localized convective instability under the isothermal sink, which is similar to the classical Rayleigh-Bernard instability. The major global effect of the roll cells is the enhancement of the heat transfer to the isothermal sink (locally by as much as a factor of 3), which explains the systematically lower core temperature predicted by the two-dimensional calculations.

The detailed velocity and temperature measurements obtained for this problem serve as a good benchmark for testing the validity of future rigorous three-dimensional codes. In the interim, the source-link method, albeit approximate, predicts circulations that are in good agreement with those measured.

INTRODUCTION

The present study of three-dimensional natural convection flow patterns in enclosures has been motivated by the desire to obtain a better understanding of the mechanisms of heat transfer and mixing in glass-melting tanks. To establish the range of variables of interest, consider the simplified schematic representation of a glass furnace in Figure 1. Solid raw materials (called the batch) are fed into a shallow tank through the so-called doghouse. The batch floats on the melt surface before dissolving and reacting to form molten glass. The energy for the conversion process is supplied by firing from above and is transferred to the reacting solids either by direct radiation to the top surfaces of the batch or by convection within the melt to the bottom of the batch. Typical glass furnace parameters in dimensional and dimensionless form are presented in Tables 1 and 2.

The problem of the overall energy mass and momentum transfer and conversion is formidable, involving the interaction of all three components—batch, melt and combustion space. However, it is expedient to decouple the investigation of the processes occurring in the batch, melt and combustion space and to represent their interface by a combination of an isothermal sink (T_s, representative of the batch), and a region of specified heat flux (q_F, representative of the heat input through the uncovered melt surface). The resulting simpler problem treated here is that of three-dimensional natural convection at high Rayleigh numbers of a large Prandtl number fluid (with a strongly temperature-dependent viscosity) in an enclosure in which the major heat source and sink are located on the top surfaces.

In an earlier study of this problem, Clomburg (1971) solved the governing equations for a two-dimensional plane representative of a longitudinal section. The validity of the computed results was tested using a glycerol model in which the side-wall heat losses were minimized (accounting for less than 1% of the total energy input) to ensure two dimensionality. The results showed that the major circulation cell was driven by the energy transfer between the source and sink on the top, and that less important circulation cells were driven by heat transfer between the source and end walls. Further, the velocities and temperature profiles near the sources and sinks exhibited the features of boundary layer flows. Although good agreement was obtained between the measured and computed velocity fields for a single longitudinal plane, the computed temperature outside the boundary layer predicted a systematically lower temperature than the experimental observation (Noble et al., 1972).

In the earlier studies, no attempt was made to investigate the transverse flow either experimentally or computationally. However, the transverse or three-dimensional component of the flow has a major influence on the residence time, refractory wear, and other parameters of practical importance in glass furnaces. The characterization of this three-dimensional motion is the major goal of this paper. To achieve this goal, complementary experimental and theoretical approaches were taken. The theoretical task exploited the fact that in glass furnaces the predominant energy flux is in the longitudinal direction, with side-wall losses accounting for about 15% of the total energy input to the melt (Table 2); the resultant predominance of the flow in the longitudinal plane permits the use of an approximate approach in which the three-dimensional problem is treated as a superposition of two-dimensional problems, as discussed in the next section.

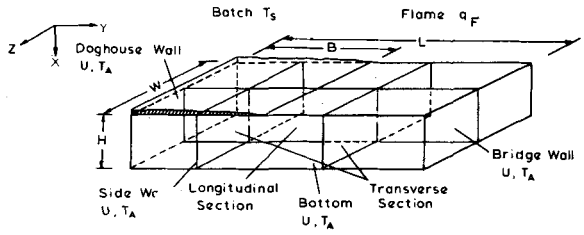

Figure 1. Simple model: geometry and boundary conditions.

TABLE 1. TYPICAL GLASS FURNACE PARAMETERS

Length	15–45 m
Width	4–11 m
Depth	0.9–1.5 m
Throughput	0.2–7 kg/s
Firing Rate	1.8–2.6 MW
Specific Heat Requirement*	2.3–3.5 MJ/kg
Glass Temperature	1,350–1,750 K
Gas Temperature	1,900–2,500 K
Top Surface Heat Flux	30–100 kW/m^2
Side-Wall Heat Flux	3–30 kW/m^2

* Theoretical enthalpy required to heat, dissolve and react batch material.

TABLE 2. DIMENSIONLESS PARAMETERS FOR GLASS FURANCES

Parameter	Definition	Fiberglas	Plate Glass	Green Glass
Rayleigh No., $R\tilde{a}$	$\frac{\tilde{g}\beta H^3 T_R}{\alpha_{eo}\nu_o}$	1.1×10^6	1.43×10^7	4.3×10^7
Prandtl No., Pr	ν_o/α_{eo}	4300	280	1660
Viscosity No., N_v'	ET_R/T_o^2	17	15	13
Batch Temp., T_s^*	T_s/T_R	1.0	0.98	0.98
Batch Coverage, C	B/L	0.5	0.15	0.5
Aspect Ratio, Long., A_L	L/H	14	47	11
Aspect Ratio, Trans., A_T	W/H	5.4	7.0	6.1
Nusselt No., Nu	UH/k_{eo}	0.03–1.0	0.02–0.14	0.05–1.7
Ambient Temp., T_A^*	T_A/T_R	0.210	0.19	0.19
Property Temp., T_o^*	T_o/T_R	1.0	1.0	1.0
Heat Flux Distribution as %				
Source		100	100	100
Batch Sink		65	45	67
Bridgewall		13	34*	7.9
Doghousewall		3	4	1
Sidewalls		13	12	15.4
Bottom		6	5	5.4
Reference Temp., T_R	K	1,480	1,640	1,640

* Including top surface cooling behind a shadow wall.

GOVERNING EQUATIONS AND APPROXIMATE METHODS OF SOLUTION

The dimensionless Boussinesq equations governing the steady flow of an incompressible Newtonian fluid in the enclosure are:

Continuity:
$$\nabla \cdot \vec{V} = 0 \tag{1}$$

Momentum:
$$\frac{1}{Pr}\vec{V}\cdot\nabla\vec{V} = -\nabla P - R\tilde{a}(T - T_0) + \nabla \cdot 2\nu\overline{\overline{\nabla\vec{V}}} \tag{2}$$

$$\vec{V}\cdot\nabla T = \nabla^2 T \tag{3}$$

$$\nu = \exp\left\{N_v\left(\frac{1}{T} - \frac{1}{T_0}\right)\right\} \tag{4}$$

$$R\tilde{a} = \frac{\tilde{g}\beta H^3 T_R}{\alpha_{eo}\nu_0}$$

$$Pr = \nu_0/\alpha_{eo}$$

$$N_v = E/T_R$$

$$\overline{\overline{\nabla\vec{V}}} = \frac{1}{2}(\nabla\vec{V} + \nabla\vec{V}^T)$$

where position, temperature, velocity and pressure have been normalized with H, T_R, α_{eo}/L, and $\mu_o\alpha_{eo}/H^2$ respectively. With appropriate boundary conditions, this set of equations describes the behavior of the fluid in the enclosure.

Two-dimensional problems are more readily solved with the elimination of pressure by taking the curl of the momentum equations (Eq. 2) and substituting Poisson's equation for vorticity to yield the fourth-order biharmonic equation in stream function, *viz.*:

$$\frac{1}{Pr}\vec{V}\cdot\nabla(\nabla^2\psi_{1z}) = -Ra\frac{\partial T}{\partial Y} + \nabla\cdot\{\nu\nabla(\nabla^2\psi_{1z})\} \tag{5}$$

where

$$\vec{V} = \nabla\times\psi_1 = \nabla\times\{0,0,\psi_{1z}\} = \vec{i}\frac{\partial\psi_{1z}}{\partial y} - \vec{j}\frac{\partial\psi_{1z}}{\partial x} \tag{6}$$

The viscous term in Eq. 5 is an approximation to the curl of the last term in Eq. 2. This form was selected because it both models the changes in the magnitude of viscosity and is readily treated with a conservative difference formulation. The effect of this simplification on the computed two-dimensional fields has been shown to be small (Curlet, 1976).

An efficient numerical code for the solution of the coupled biharmonic and energy equations with general boundary conditions was written by Clomburg (1971). Conservative finite difference analogs to these equations (with allowance for variable zoning) were solved by an iterative alternating direction implicit procedure.

To utilize this algorithm to obtain approximate three-dimensional fields, a method was devised for approximating the solution of three-dimensional problems by that for coupled two-dimensional problems (Won, 1974). The basic concept rests on the idea that the flow developed in a longitudinal plane will be dominant to satisfy the imposed thermal boundary conditions. Then, it is possible to divide the temperature and velocity fields into two parts: a longitudinal and a transverse contribution. This technique, termed the source-sink method, is based on the following simplifications:

(1) The fluid has a high Prandtl Number, enabling the nonlinear advective terms in the momentum equation to be neglected.

(2) The velocity field may be represented as the sum of two orthogonal velocity vectors, each satisfying its own continuity equation.

Thus:

$$\vec{V}_{x,y,z} = \vec{V}_{x,y} + \delta\vec{v}_{x,y,z} \tag{7a}$$

$$= \vec{i}\{u + \delta u\} + \vec{j}\{v\} + \vec{k}\{\delta w\} \tag{7b}$$

where,

$$\vec{V}(x,y) = \frac{1}{A_T}\int_0^{A_T}\vec{V}\,dz \tag{8}$$

$$\nabla\cdot\vec{V} = \nabla\cdot\vec{V} + \nabla\cdot\delta\vec{v} = 0 \tag{9}$$

(3) The underlined terms in the vorticity transport equation below, which represent the diffusion of vorticity, are small and may be neglected. Since these are all tangential (y-axis) rather than normal gradients under the top surface, they can be expected to be small. With these assumptions, the three-dimensional vorticity transport equations become:

$$\vec{i} \qquad \underline{-\nabla^4\psi_{2x}} = 0 \tag{10}$$

$$\vec{j} \qquad Ra\frac{\partial T}{\partial z} + \nabla_{ik}^4\psi_{2y} + \underline{\frac{\partial^2}{\partial y^2}\nabla^2\psi_{2y}} = 0 \tag{11}$$

$$\vec{k} \qquad -Ra\frac{\partial T}{\partial y} + \nabla_{ij}^4\psi_{1z} - \underline{\nabla^2\psi_{2z}} = 0 \tag{12}$$

where,

$$-\nabla^2\psi_{1z} = \frac{\partial v}{\partial x} - \frac{\partial u}{\partial y} \tag{13}$$

$$-\nabla^2\psi_{2x} = \frac{\partial\delta\omega}{\partial y} \tag{14}$$

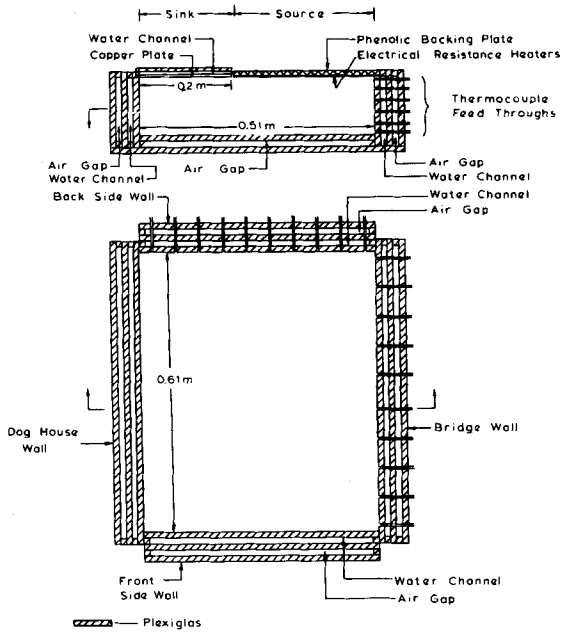

Figure 2. Experimental model tank.

$$-\nabla^2\psi_{2y} = \frac{\partial\delta u}{\partial z} - \frac{\partial\delta\omega}{\partial x} \tag{15}$$

$$-\nabla^2\psi_{2z} = -\frac{\partial\delta u}{\partial y} \tag{16}$$

Neglecting the underlined terms reduces the problem to two biharmonic equations (Eqs. 11 and 12) representing flow in two othogonal planes. In the derivation above, viscosity has been assumed constant; however, this constraint may be relaxed and the effect of changes in viscosity may be included by allowing for the variation in Rayleigh number with temperature.

A suitable decomposition of the coupled energy equation for the two orthogonal planes is obtained by writing Eq. 3 as:

$$\vec{V}\cdot\nabla T - \nabla^2_{ij}T = -\frac{\partial^2 T}{\partial x^2} - \{\delta\vec{v}\cdot\nabla T - \nabla^2_{ik}T\} \equiv SI_L \tag{17}$$

$$\delta\vec{v}\cdot\nabla T - \nabla^2_{ik}T = -\frac{\partial^2 T}{\partial x^2} - \{\vec{V}\cdot\nabla T - \nabla^2_{ij}T\} \equiv SI_T \tag{18}$$

The righthand side of Eqs. 17 and 18 represent the energy transfer between the x-y and y-z planes and define the source-sink functions which form the coupling between the two planes. These sets of orthogonal equations (Eqs. 12 and 17; Eqs. 11 and 18), coupled by the source-sink term, may be solved using the two-dimensional algorithm for different planes to yield an approximate solution for the three-dimensional convective field.

For good resolution of the two-dimensional flow, the boundary layer under the top surface must be adequately zoned (Noble et al., 1972). Fine zoning is also required near the side walls where roll cells are formed. For calculations in the longitudinal (xy) plane, 20 vertical, and 46 axial zones were used. For calculations in the transverse (xz) plane, the same vertical grid spacing was selected, with 23 horizontal grid points under the source, and 53 horizontal grid points under the sink. The variation in grid spacing is given by Curlet (1976).

It should be noted that the basic separation of the equations for the temperatures and velocity fields is not related to a perturbation analysis. Recently, this separation technique was extended to include momentum source and sink terms (Mercier and Deville, 1979). However, the refined technique, called the weak coupling approximation, seems to have a drawback in placing a restriction of no vertical motion change between the orthogonal planes.

EXPERIMENTAL APPROACH

A companion experimental program was performed to both verify the source-sink method of analysis and to serve as a benchmark for testing the validity of three dimensional numerical codes.

A simple experimental model with glycerol (Prandtl number $\sim 5 \times 10^3$) as the modeling fluid was designed for a Rayleigh number, $Ra \sim 10^7$ and a viscosity number of $N_V' \sim 16$, approximating the conditions of interest in glass melts. The model consisted of a multiwalled Plexiglas box, Figure 2, in which the heat input (88 W) was provided by electrical resistance heaters, while the isothermal sink on the top (~27°C) was a water-cooled copper plate. Additional heat losses through the side and end walls were controlled by water cooling.

Temperature measurements within the tank were made with two orthogonal banks of copper-constantan thermocouples (5 mil diameter) whose positions were recorded photographically or with a cathetometer.

To visualize the flow, neutrally buoyant anthracene particles were illuminated with a planar light source, and both streak and multiple exposure photographs were taken of longitudinal and transverse planes. Velocities were determined from the latter photographs by determining the particle coordinates at successive time intervals.

Four experimental runs were performed to investigate:

(a) Two-dimensional longitudinal flow with minimal sidewall heat loss (~1.0% of total heat input) (Runs 3, 4 and 5).

(b) The effect of increased side-wall heat loss (15% of total heat input) on the two-dimensional flow (Run 6).

(c) The transverse convective flows driven by the sidewall heat loss (Run 6).

The dimensionless parameters of these four runs and their energy balances are shown in Tables 3 and 4 respectively.

Overall circulation patterns (from streak photographs) and velocity profiles (from multiple-exposure photographs) were obtained for at least three longitudinal and four transverse planes for each run. In addition, temperature profiles in the boundary layer and core regions of both planes were measured.

RESULTS AND DISCUSSION

The experimental results illustrating the major features of the convective flow are presented and compared with computed results obtained using the source-sink method. To facilitate the presentation of the data, the locations of the longitudinal and transverse planes discussed are shown schematically in Figure 3. Also given in Figure 3 are the numbers of the figures wherein the experiments and computational results for each transverse and longitudinal

TABLE 3. DIMENSIONLESS PARAMETERS FOR EXPERIMENTAL RUNS*

Parameter	Definition	Run #3	Run #4	Run #5	Run #6
Rayleigh No., $R\tilde{a}$	$\tilde{g}\beta H^3 T_R/\alpha_{es}\nu_s$	5.0×10^7	5.1×10^7	4.21×10^7	4.21×10^7
Prandtl No., Pr	ν_s/α_{es}	4.95×10^3	4.85×10^3	5.9×10^3	5.9×10^3
Viscosity No., N_v'	ET_R/T_s^2	16.35	16.33	16.92	16.92
Nusselt No., Nu	UH/k_{es}	9.22	9.22	9.22	9.22
Doghouse Water Temp., θ_{DHW}	$(T_{DHW} - T_s)/T_R$	−0.0354	−0.0357	−0.0185	−0.0176
Bridgewall Water Temp., θ_{BW}	$(T_{BW} - T_s)/T_R$	−0.0360	−0.0367	−0.0232	−0.0233
Sidewall Water Temp., θ_{SW}	$(T_{SW} - T_s)/T_R$	—	—	—	−0.0236
Ambient Air Temp., θ_A	$(T_A - T_s)/T_R$	−0.0335	−0.0275	−0.0110	−0.0137
Reference Temp., T_r	$q_F H/k_{es}$, K	223	222	224	228

* All properties evaluated at batch sink temperature T_s.

TABLE 4. EXPERIMENTAL ENERGY BALANCES

Run	#3		#4		#5		#6	
	Q,W	%	Q,W	%	Q,W	%	Q,W	%
Output								
Batch Sink	66.20	70.8	63.3	68.3	61.30	77.8	66.20	69.6
Bridgewall	11.70	12.5	12.9	13.9	11.14	14.1	12.50	13.2
Doghouse Wall	8.79	9.4	8.0	8.6	4.81	6.1	4.28	4.5
Front Side Wall[1]	0.64	0.7	0.5	0.5	0.21	0.3	7.36	7.7
Back Side Wall[1]	0.64	0.7	0.5	0.5	0.21	0.3	7.27	7.6
Bottom Surface[2]	3.43	3.7	2.7	2.9	1.13	1.4	1.41	1.5
Total Output	91.40	97.8	87.9	94.8	78.80	99.9	99.00	104.1
Input from Heaters	93.50	100.0	92.7	100.0	78.90	100.0	95.10	100.0
Discrepancy								
Input-Output	2.10	2.2	4.8	5.2	0.10	0.1	−3.90	−4.1

[1] Estimated for Runs 3, 4, 5.
[2] Estimated for all runs.

plane may be located.

For the computational results presented, the source-sink method was applied in the following manner. First, the center-line longitudinal plane was simulated with the use of uniformly distributed sinks to allow for the side wall heat loss. Then, three transverse planes (one under the source and two under the isothermal sink) were simulated with the source-sink distribution from the longitudinal plane. Finally, the energy distributions from these transverse planes were crudely applied to appropriate regions and used to generate improved results for the longitudinal plane. Although only one longitudinal and three transverse planes were used to limit the computational effort, this approximate treatment was found to be sufficient to identify and characterize the important features of the flow. The conditions simulated were the cases of minimal side-wall heat loss (Run 5), and side wall heat losses corresponding to 15% of the energy input (Run 6).

LONGITUDINAL FLOW FIELD

Clomburg (1971) had previously characterized the general features of the flow in a single longitudinal plane of a similar model. Here, the dominance of the two-dimensional boundary layer flow in such systems has been confirmed by the examination of several longitudinal planes, one of which (at $z^* = 1.2$) is shown in Figure 4, where streak lines from Run 5 (side-wall heat loss 0.6%) are depicted and compared with computed streamlines. In both the experimental and computed fields, a dominant circulation cell is set up to convect energy from the source to the isothermal sink, while smaller circulation cells are set up adjacent to the end walls as a consequence of the lesser heat losses through these walls. Notice that a small recirculation cell was set up under the top surface in the run due to a local temperature perturbation resulting from the failure of one of the six strip resistance heaters on the top surface.

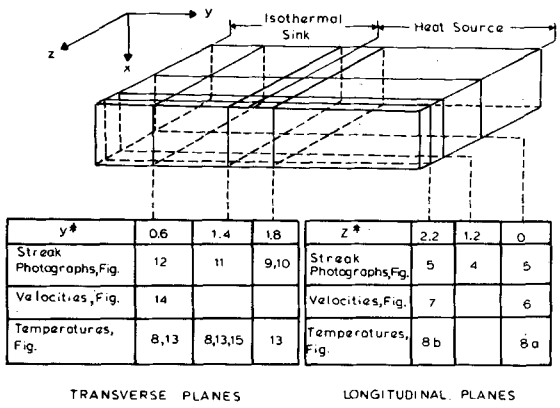

Figure 3. Location of longitudinal and transverse planes (dimensionless coordinates y^* and z^* are normalized with model depth 0.127 m).

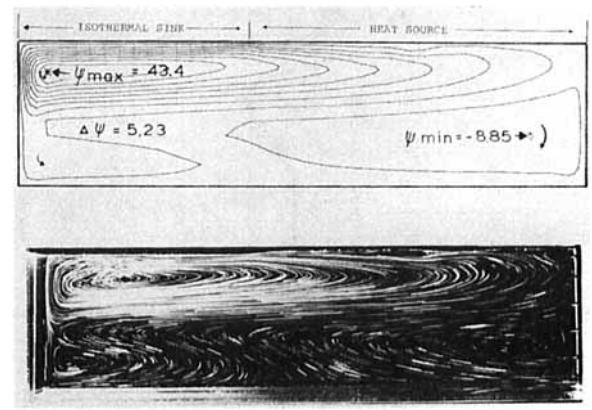

Figure 4. Experimental streaklines and computed streamlines for longitudinal plane for Run 5 (streak photograph taken at $z = 0.15$ m, $z^* = 1.2$, exposure time 20 minutes).

The characteristics of the dominant two-dimensional motion are maintained *even* when the side-wall heat loss is increased to 15% of the total heat input. It is demonstrated by the longitudinal streak at two different planes ($z^* = 0$ and $z^* = 2.2$) shown in Figure 5. More cogent and quantitative demonstration of this continued dominance is evident in comparing the longitudinal velocity profiles for the two z planes presented in Figure 6 and 7. (The computed curves are the same in both figures so that differences in the position of the data points relative to the curves provides a measure of the variation in velocity between different z planes.) The only significant difference in the velocities is in the core region ($x^* > 0.2$, i.e., $x > 25$ mm) as is also evident in the streak in Figure 5.

VERTICAL TEMPERATURE DISTRIBUTIONS

Similar behavior is evident in the temperature fields. The ex-

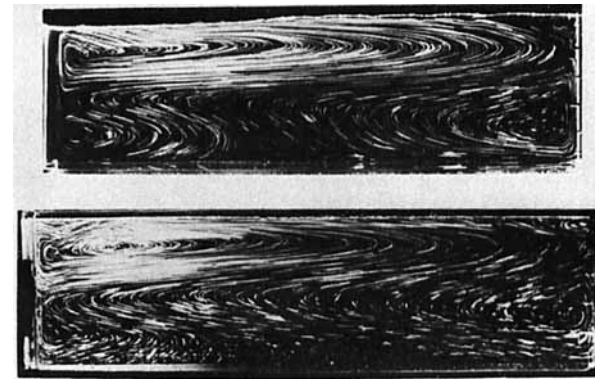

Figure 5. Experimental streaklines for two longitudinal planes for Run 6 (top photograph: $z = 0$, $z^* = 0$; bottom photograph: $z = 0.28$ m, $z^* = 2.2$, exposure time 20 minutes).

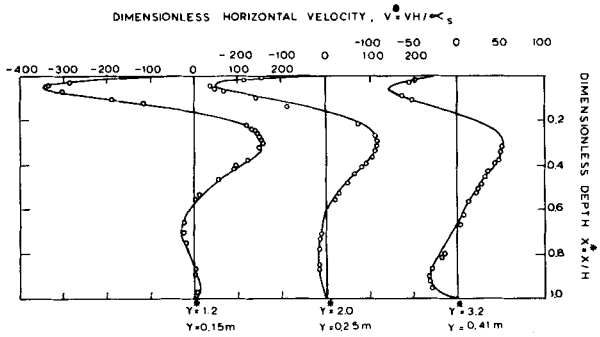

Figure 6. Comparison of experimental and computed longitudinal velocity profiles for Run 6 at $z^* = 0$.

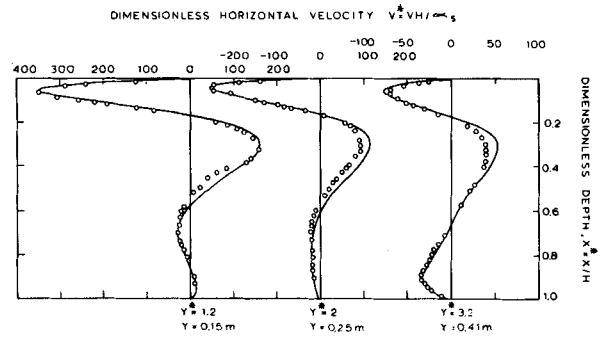

Figure 7. Comparison of experimental and computed longitudinal velocity profiles for Run 6 at $z^* = 2.2$.

perimental temperatures at the center line are in good agreement with the values computed using the source-sink method (Figure 8a). The predicted temperatures are slightly higher {$\Delta\theta \sim 0.002$ (~ 0.44°C)}, a discrepancy probably caused by the limited number of planes used for the source-sink method. Near the side wall ($z^* - 2.2$, Figure 8b), the influence of the heat loss is evident in the lower core temperatures measured.

A novel feature of the flow evident in the streak photographs is the instability (the crossing streak lines) occuring under the isothermal sink. This phenomenon, analogous to Rayleigh-Benard cells, is caused by the unstable temperature gradient in the developing thermal boundary layer flow under the batch. Their principal influence on the overall two-dimensional circulation is the enhancement of the heat transfer to a section of the isothermal sink. This convective instability has been the subject of separate study (Won, 1979).

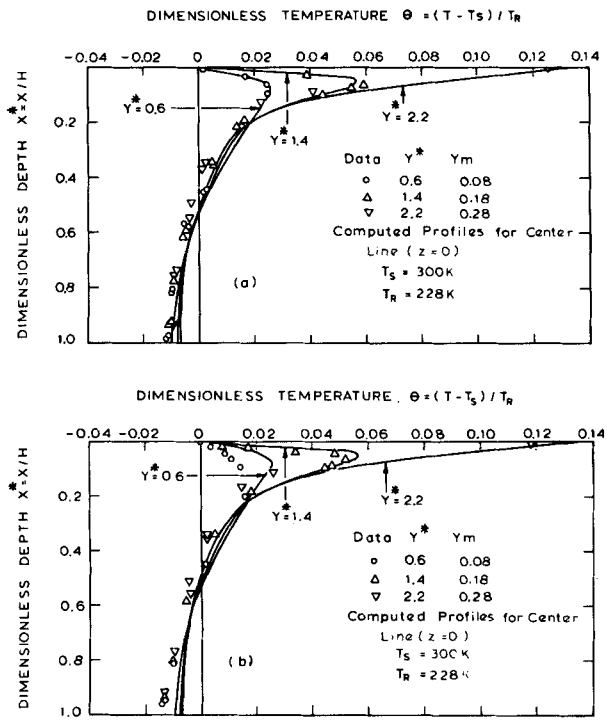

Figure 8. Comparison of experimental and computed temperature profiles for Run 6 at (a) $z = 0$, $z^* = 0$; (b) $z = -0.28$ m, $z^* = -2.2$.

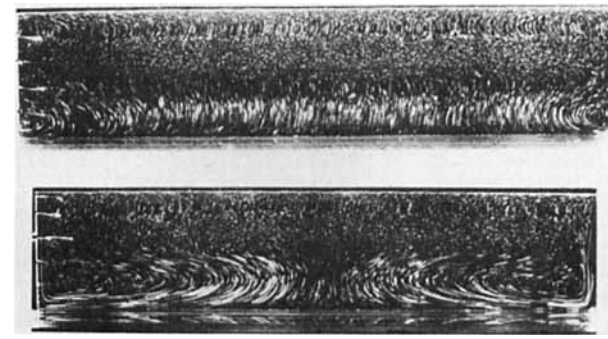

Figure 9. Experimental streaklines for transverse planes for Runs 5 and 6 (top: runs at $y = 0.235$ m, $y^* = 1.85$; bottom: run 6 at $y = 0.229$ m, $y^* = 1.8$).

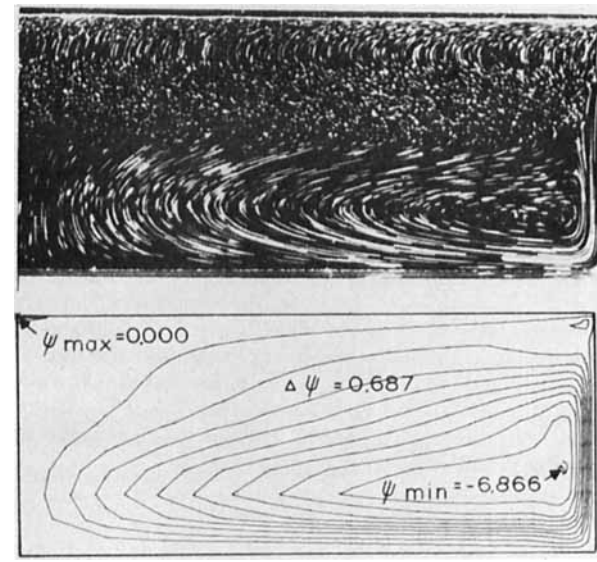

Figure 10. Experimental streaklines and computed streamlines for transverse half plane under the source (Run 6: $y^* = 1.8$; exposure time 20 minutes).

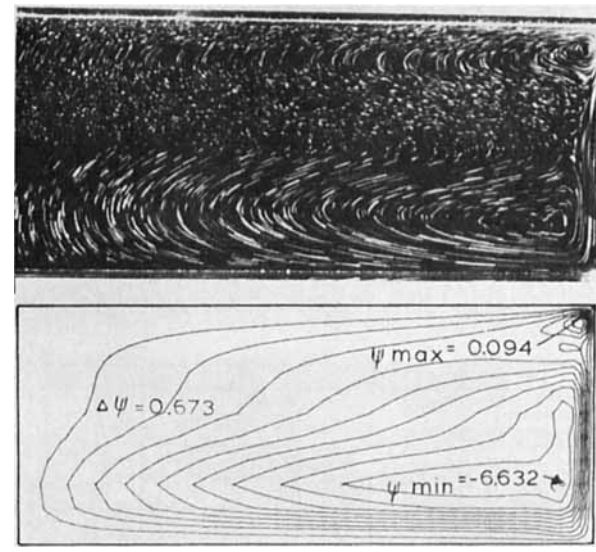

Figure 11. Experimental streaklines and computed streamlines for transverse half plane under the sink (Run 6: $y^* = 1.4$; exposure time 15 minutes).

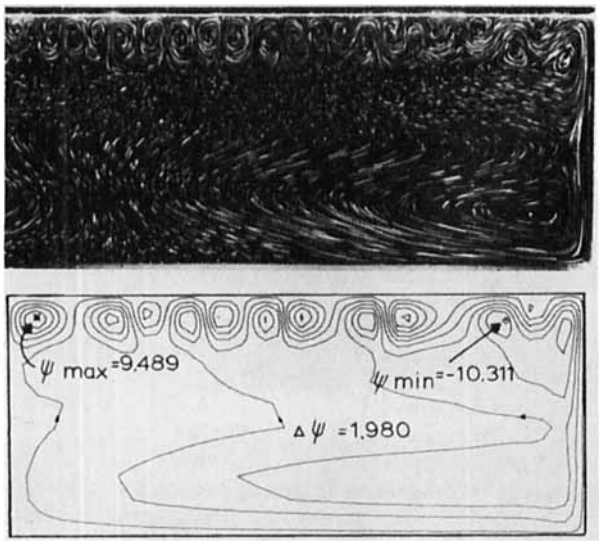

Figure 12. Experimental streaklines and computed streamlines for transverse half plane under the sink—illustrating roll cells (Run 6: $y^* = 0.6$; exposure time 15 minutes).

TRANSVERSE FLOW AND TEMPERATURE FIELDS

The transverse temperature and velocity fields have been characterized experimentally both to complete the specification of the three-dimensional field and to provide data for a more stringent test of the source-sink method.

The effect of increasing the side wall heat loss [from 1% (Run 5) to 15% (Run 6) of the total heat loss] is graphically depicted in the transverse streak shown in Figure 9. While the upper part (Run 5) reemphasizes the basic two dimensionality of the longitudinal flow, the lower part (Run 6) shows the significant effect of the side-wall heat loss on the flow in the core region. (The short streak lines indicate the predominantly longitudinal flow.) The observed circulation for three different transverse half planes (Figure 3) are depicted in Figures 10, 11 and 12 and compared with streamlines generated using the source-sink method; the corresponding computed isotherms are shown in Figure 13. Under the heat source (Figure 10) the major circulation occurs in the core region and the location of the eye of this cell is determined by the boundary layer flow down the side wall. However, under the isothermal sink the adverse temperature gradient in the developing thermal boundary layer produces an additional circulation cell (Figure 11) close to the top surface. Ultimately, as the thermal boundary layer thickens, the onset of the roll cells occurs and they grow until they occupy the entire hydrodynamic boundary layer (Figure 12). The salient features of these circulations are well predicted by the source-sink method as indicated in the computed isotherms and streamlines for these transverse planes. Under the isothermal sink, the only driving force for the transverse circulation is supplied by the distributed sources, as is evident by the location of the maximum temperature within the fluid.

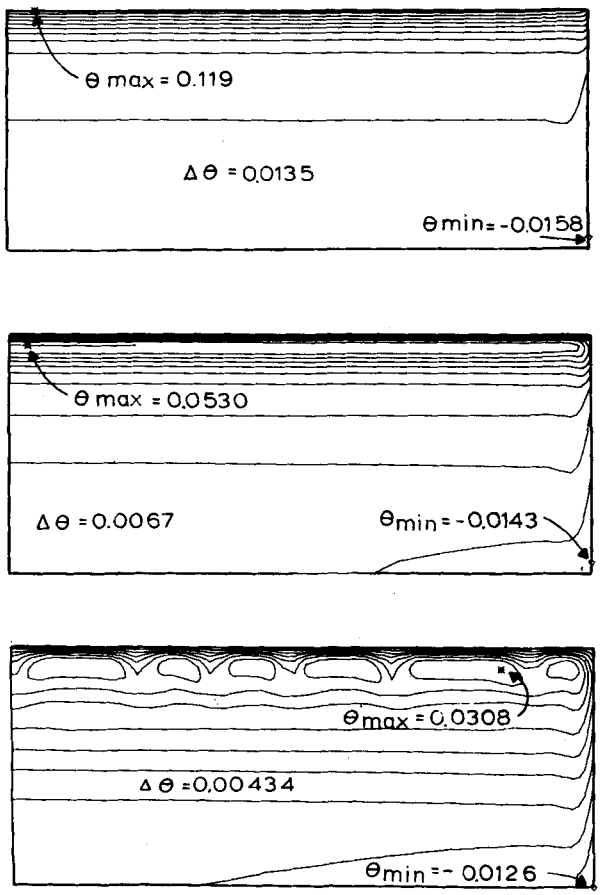

Figure 13. Computed isotherms for three transverse planes [(a) $y^* = 1.8$, (b) $y^* = 1.4$, (c) $y^* = 0.63$].

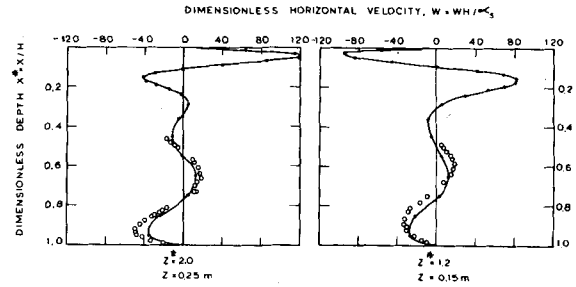

Figure 14. Comparison of experimental and computed transverse velocity profiles for Run 6 at $y^* = 0.6$.

Experimental and computed horizontal transverse velocities are compared in Figure 14. The agreement is good, particularly considering the rather coarse zoning used for the core (the curves

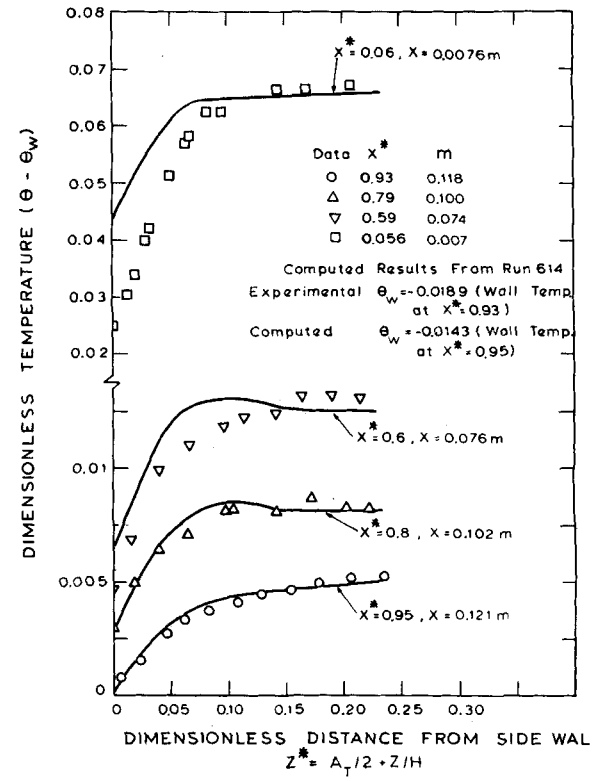

Figure 15. Comparison of experimental and computed temperature profiles in sidewall boundary layer at $y = 0.178$ m, $y^* = 1.4$.

represent computed velocities and the open circles measured velocities), and the limited number of planes used in the source-sink method. The change in the sign of the computed velocities close to the top surface is caused by traversing through different roll cells.

The measured and computed temperature profiles at different depths in the boundary layers near the side walls are compared in Figure 15. All the temperatures are expressed as a difference with the inside wall temperature θw of the deepest profile. (The boundary condition at this wall is $\partial\theta/\partial x^* = Nu(\theta - \theta_{SW})$, where $Nu = 9.22$ and $\theta_{SW} = -0.0236$ (experimental and computed). Both the relative heat flux and the boundary layer thickness are in reasonable agreement, though less close to the top surface because of the large temperature gradients there.

The comparison of the experimental and computed data presented here represent a critical test of the source-sink method since the distributed heat sources and sinks are the major energy terms. The agreement found is surprisingly good in view of the crude application of the method—only one longitudinal and three transverse planes and one iteration between the planes. These factors probably account for the discrepancy between the computed temperatures at the center lines of the transverse planes and the equivalent ones in the longitudinal plane; this difference was $\Delta\theta \sim 0.005$ (~1.1 C or 5% of the overall temperature difference).

ACKNOWLEDGMENT

The research at M.I.T. on the modeling of circulation within glass tanks was initiated by H. C. Hottel, and the authors are indebted to him for his valuable suggestions and encouragement. Financial support by Owens-Illinois, PPG Industries, Brockway Glass and the National Science Foundation is gratefully acknowledged.

NOTATION

A_L = longitudinal aspect ratio, L/H
A_T = transverse aspect ratio, W/H
B = *batch length*
C = batch coverage, B/L
E = viscosity power constant, Eq. 4
g = acceleration due to gravity
H = model depth (x dimension)
$\vec{i},\vec{j},\vec{k}$ = unit vectors for Castesian coordinate system, Figure 1
k = thermal conductivity
k_e = effective thermal conductivity, allowance for radiation
L = model length (y dimension)
Nu = Nusselt number, UH/k_e
N_v' = modified (linearized) viscosity number, ET_R/T_s^2
P = pressure
Pr = Prandtl number $\mu C_p/k_e$
Q = total heat flux
q_F = heat flux density for heat source
Ra = Rayleigh number, $\dfrac{\vec{g}\beta H^3 T_R}{\alpha_{eo}\nu_o}$
SI_L = source sink term for longitudinal planes, Eq. 17
SI_T = source sink term for transverse planes, Eq. 18
T = temperature
T_A = ambient temperature
T_o = temperature for property evaluation
T_s = isothermal sink or batch temperature
T_R = reference temperature, $T_R = q_F H/k_e$
U = overall heat transfer coefficient
u = x velocity component
δu = x velocity component (transverse)
$\vec{V}$ = velocity vector
$\vec{V}$ = longitudinal velocity vector, Eq. 7a
$\delta\vec{V}$ = transverse velocity vector, Eq. 7
v = y velocity component
W = model width (z dimension)
$w,\delta w$ = z velocity component
x,y,z = Cartesian coordinates, Figure 1

Greek Letters

α = thermal diffusivity, $k/\rho C_p$
α_e = effective thermal diffusivity, $k_e/\rho C_p$
β = coefficient of volumetric expansion
θ = dimensionless temperature, $(T - T_s)/T_R$
μ = viscosity
ν = kinematic viscosity, μ/ρ
ρ = density
$\vec{\Psi}$ = vector potential, $\vec{V} = \nabla \times \vec{\Psi}$
$\psi_{1x},\psi_{1y},\psi_{1z}$ = components of vector potential, $\vec{\Psi}_1$
$\psi_{2x},\psi_{2y},\psi_{2z}$ = components of vector potential, $\vec{\Psi}_2$

Vector Symbols and Operator

$\nabla\vec{V}$ = velocity gradient tensor, $\nabla\vec{V}^T$ its transpose
$\overline{\overline{\nabla\vec{V}}}$ = rate of deformation tensor
∇ = gradient operator
$\nabla\cdot$ = divergence operator
∇x = curl operator
∇^2 = Laplacian operator
∇^4 = biharmonic operator

Superscripts

$\rightarrow$ = vector quantity
$*$ = dimensionless quantity, normally dropped

Subscripts

A = ambient conditions
max = maximum value
min = minimum value
o = property evaluated at T_o
R = reference quantity
s = property evaluated at T_s
i,j,k = specific Cartesian coordinates for operator, e.g.,

$$\nabla_{ij}^2 = \frac{\partial^2}{\partial x^2} + \frac{\partial^2}{\partial y^2}$$

w = temperature at wall
BA = batch or isothermal sink
BW = bridgewall
DHW = doghousewall
FSW = front side wall
BSW = back side wall
BOT = bottom

LITERATURE CITED

Catton, I., and D. K. Edwards, "Effects of Side Walls on Natural Convection between Horizontal Plates heated from Below," *J. Heat Transfer*, **89C**, 295 (1967).

Clomburg, Jr., L. A., "Mathematical and Experimental Modeling of the Circulation Patterns in Glass Melts," Sc.D. Thesis, M.I.T., Cambridge (1971).

Curlet, N. W. E., "Experimental and Numerical Modeling of Three Dimensional Natural Convection in an Enclosure," Sc.D. Thesis, M.I.T. Cambridge (1976).

Mallinson, G. G., and G. de Vahl Davis, "The Method of the False Transient for the Solution of Coupled Elliptic Equations," *J. Comp. Phy.*, **12**, 435 (1973a).

Mercier, P., and M. Deville, "Three Dimensional Numerical Study of Glass Flow in a Forehearth," *Glasstechn. Ber.*, **52**, 131 (1979).

Moore, D. R., and N. O. Wiss, "Two Dimensional Rayleigh-Benard Convection," *J. Fluid Mech.*, 58(2), 289 (1973).
Noble, J. J., L. A. Clomburg, A. F. Sarofim, and H. C. Hottel, Mathematical and Experimental Modeling of the Circulation Patterns in Glass Metals," *J. Heat Transfer*, 5, 149 (1972).
Ozoe, H. H. Sayama, and S. W. Churchill, "Natural Circulation in an Inclined Rectangular Channel Heated on one Side and Cooled on the Opposing Side," *Int. J. Heat Mass Trans.*, 17, 1209 (1974).
Won, K. J., "Experimental and Theoretical Study of Convective Instability in an Enclosure," Sc.D. Thesis, M.I.T., Cambridge (1979).
Won, K. J., "Simulation of Glass Melter Performance," S.M. Thesis, M.I.T., Cambridge (1974).

Manuscript received November 2, 1981; revision received April 5, and accepted April 15, 1983.

Critical Point Measurements on Nearly Polydisperse Fluids

The critical temperatures, pressures and volumes of several mixtures containing CO_2, C_2H_6, C_3H_8, and C_4H_{10} have been measured using a heavy walled, variable volume, cylindrical glass vessel. In each mixture the relative proportions of the three hydrocarbon solutes to one another were changed; total solute mole fraction never exceeded 0.1. A detailed study of the mixture $CO_2 + C_3H_8$ shows that the critical temperature exhibits a minimum at a C_3H_8 mole fraction of 0.0265. Our mixture data are analyzed using a polydisperse model of dilute solutions.

G. MORRISON and J. M. KINCAID

Thermophysics Division
National Bureau of Standards
Washington, DC 20234

SCOPE

There now exist large collections of information about the properties of binary mixtures, such as the recent bibliographic collection of Hicks (1978), the classic data collection by Timmermans (1959), or the bibliographic collection of Wichterle et al. (1973, 1976, 1979). As the number of components in the mixture increases, the amount of information drops rapidly. Nonetheless, complex mixtures, those that contain dozens or even hundreds of components, are both common and, in some cases, economically important—industrial reaction mixtures and petroleum, to name two examples. The complexity of such materials makes all but the most narrow studies of their properties prohibitive. One way of approaching the problem of complex mixtures is to treat them as a special case of mixtures with an infinite number of components. In such a mixture, each molecular species is identified by the value of a continuous parameter, which may be multidimensional in character, and is inevitably connected to the physical properties of the species. Thus, as one would expect intuitively, species with similar values of the identification parameter would have similar properties. Unlike a mixture of discrete species, however, in which the composition would be characterized by a discrete set of values drawn from all possible values of the identification parameter, the infinite-component mixture would have components described by every possible value of that discriptor. Such a mixture is said to be "polydisperse." This kind of mixture model has been used extensively in the theory of high-polymer solutions and has been addressed at length for that special application by Flory (1978), Koningsveld (1969), and Scott (1952). This model has also been applied to hard-sphere mixtures by Blum and Stell (1979) and Vrij (1978). Recently the thermodynamics of the polydisperse mixture has been discussed by Salacuse (1978), Dickinson (1981), Kehlen (1981), and Gualtieri, Kincaid and Morrison (1982).

A special class of polydisperse mixture is one in which one component dominates the composition—acting as a solvent—and the remaining, infinite number of components are present collectively at a low concentration—a solute. In collaboration with Gualtieri (1982) we have described the thermodynamics of such a mixture in detail. In this paper we examine the critical properties of a similar, but far simpler, mixture, in which near-critical CO_2 is the solvent and various mixtures of ethane, propane and n-butane are the solute. The critical densities and temperatures of the mixtures are measured at 0.0, about 2.5 mol %, and about 9.0 mol % overall alkane composition. We have analyzed the data in two ways: first, by investigating the connection between the properties of the binary mixtures—that is, carbon dioxide and a single alkane—and the more complex mixtures; and, second, by modeling the mixture using our earlier analysis of the polydisperse impurity problems. For the second analysis, we have used the van der Waals free energy, the customary mixing rules for the unlike molecular interactions, a scheme for evaluating the molecular identification parameter, and have shown how information derived from the behavior of each solute component in the solvent leads to a scale for the identification parameter.

CONCLUSIONS AND SIGNIFICANCE

The critical loci of the binary mixtures $CO_2 + C_2H_6$, $CO_2 + C_3H_8$, and $CO_2 + C_4H_{10}$ at low alkane composition exhibit a simple dependence upon the alkane mole fraction. The heretofore unmeasured shallow minimum in the $CO_2 + C_3H_8$ critical temperature, Figure 2a, can be viewed as a natural consequence of the transition from $CO_2 + C_2H_6$ to $CO_2 + C_4H_{10}$ behavior. At low concentrations of a mixed solute, we show that the components act separately and that, under certain restrictive conditions, the effect of the mixed solute on the critical point of the mixture can be predicted by knowing the separate effect of each component of the solute. The analysis of the data in terms of the van der Waals binary mixture model shows clearly that effective